Scalable Ultrasmall Three-Dimensional Nanowire Transistor Probes for Intracellular Recording

Citation

Permanent link

Terms of Use

Share Your Story

Title: Scalable ultrasmall three-dimensional nanowire transistor probes for intracellular recording

Authors: Yunlong Zhao[1,2†], Siheng Sean You[1†], Anqi Zhang[1†], Jae-Hyun Lee[1,3], Jinlin Huang[1] and Charles M. Lieber[1,4,5]*

Affiliations:

[1] Department of Chemistry and Chemical Biology, Harvard University, Cambridge, Massachusetts 02138, USA

[2] Advanced Technology Institute, University of Surrey, Guildford, Surrey GU2 7XH, UK

[3] Center for Nanomedicine, Institute for Basic Science (IBS), Yonsei-IBS Institute, Yonsei University, Seoul 03722, Republic of Korea

[4] Center for Brain Science, Harvard University, Cambridge, Massachusetts 02138, USA

[5] John A. Paulson School of Engineering and Applied Sciences, Harvard University, Cambridge, Massachusetts 02138, USA

†These authors contributed equally to this work.

*e-mail: cml@cmliris.harvard.edu

Abstract

New tools for intracellular electrophysiology that push the limits of spatiotemporal resolution while reducing invasiveness could provide a deeper understanding of electrogenic cells and their networks in tissues and push progress towards human-machine interfaces. While significant advances have been made in developing nanodevices for intracellular probes, current approaches exhibit a tradeoff between device scalability and recording amplitude. We address this challenge by combining deterministic shape-controlled nanowire transfer with spatially-defined semiconductor-to-metal transformation to realize scalable nanowire field-effect transistor probe arrays with controllable tip geometry and sensor size, which enable recording of up to 100 mV intracellular action potentials from primary neurons. Systematic studies on neurons and cardiomyocytes show that controlling device curvature and sensor size is critical for achieving high amplitude intracellular recordings. In addition, this device design allows for multiplexed recording from single cells and cell networks and could enable future investigations of dynamics in the brain and other tissues.

33   **Main text**

34   Developing new tools that enable reproducible high spatial-temporal resolution recording

35   of intracellular potential, while maintaining the capability for device scalability, are key goals for

36   advancing electrophysiology studies of electrogenic cells and cell networks[1-4]. Patch-clamp

37   electrodes have been the "gold standard" for cell electrophysiology for decades, where it has

38   been shown that accurate recording of the intracellular potential requires a high resistance seal

39   against the cell membrane and low resistance between the recording element and the cell

40   interior[5,6]. Recent studies have focused on several solid-state nanodevice architectures, including

41   nanowire-based structures for optical neuronal stimulation[7,8], scalable on-chip micro/nano-

42   structured electrode arrays[9,10] for attenuated intracellular recording via electroporation[11,12] and/or

43   optoporation[13,14], and three-dimensional nanowire field effect transistor probes for intracellular

44   recording of single cells[15,16]. Nanowire probes have recorded cardiac intracellular action

45   potentials with amplitudes comparable to those recorded with patch-clamp micropipettes[15,16], but

46   have relied on 1-by-1 fabrication that has been difficult to scale-up.   For   solid-state

47   nanoprobes to achieve comparable recording signal-to-noise and amplitude to patch clamp, the

48   nanodevice must achieve direct contact of the recording element with the intracellular solution

49   without significantly disturbing the cell membrane[2, 9]. Fulfilling these criteria requires

50   understanding of the size, geometry, mechanical, and biochemical factors present at the cell

51   membrane/nanodevice interface. Recent work suggests that nanoscale size and geometry play a

52   key role in the interaction between the nanostructure and the cell membrane[17,18]. For example,

53   nanoscale membrane curvature elevates the local concentration of endocytosis related

54   proteins[17,18], influences the conformation and activity of transmembrane proteins[19], and is

55   hypothesized to recruit a sequence of proteins leading to membrane fission[20]. Building on these

56 studies, we hypothesize that inducing appropriate nanoscale curvature on the cell membrane via

57 rational device design will facilitate probe internalization and enable intracellular recording.

58   Here, we investigate how size and geometry of nanoprobes influence intracellular

59 recording by fabricating scalable three-dimensional U-shaped nanowire field effect transistor (U-

60 NWFET) arrays in which both the radii of curvature (ROC) and active sensor sizes are controlled

61 (Fig. 1a). To investigate how these design factors affect electrophysiological recording, arrays of

62 U-NWFET probes fabricated from 15 nm diameter p-type Si nanowires with ROC from $0.75 - 2$

63 µm and active channel lengths from $50 - 2000$ nm were used to probe cultured primary neurons

64 and human cardiomyocytes. Schematically, we ask whether probes with the smallest ROC and

65 sensor size (Fig. 1b(i)) can facilitate recording full amplitude intracellular action potentials and

66 subthreshold features, whereas increases in the ROC and detector sizes (Fig. 1b(ii)) would lead

67 to recording smaller amplitude intracellular-like or extracellular action potential peaks.

68 **U-shaped nanowire probe fabrication and characterization**

69   Our strategy for producing reproducible arrays of U-NWFET probes with controlled

70 ROC and active FET channel lengths or detector sizes involves two key techniques (see Methods

71 for details). First, large-scale, shape-controlled deterministic assembly[21] is used to produce U-

72 shaped nanowire arrays from 15 nm diameter Si nanowires with controllable ROC on top of

73 Si_3N_4 patterns (Fig. 2a(i); Supplementary Fig. 1a-e). Metal contacts are then deposited and

74 passivated by an upper Si_3N_4 layer (Supplementary Fig. 1f). Second, we exploit spatially-defined

75 solid-state transformation[22] to convert Si nanowire segments underneath and adjacent to Ni

76 diffusion layer to metallic NiSi, thereby producing controlled length of FET sensing elements at

77 the tips of the U-shaped nanowire probes (Fig. 2a(ii); Supplementary Fig. 1g). Last, etching of

78 the sacrificial layer allows the probes to bend upward due to interfacial strain in the metal

79 interconnects (Fig. 2a(iii))[15], yielding probe arrays with up to 4 addressable U-NWFETs per

80 bend-up probe arm (Supplementary Fig. 1h).

81   Optical microscopy and scanning electron microscopy (SEM) were used to characterize

82 key steps in the U-NWFET probe fabrication flow. Optical microscopy images of the patterned

83 bottom passivation layer and U-shaped trenches that set the ROC during nanowire assembly

84 (Supplementary Fig. 2a,b) as well as three probes with U-shaped nanowires, metal contacts and

85 top passivation layer (Fig. 2b) are indicative of the deterministic parallel assembly of U-shaped

86 nanowire probes with defined ROC. Composition-sensitive SEM images of U-NWFETs

87 following annealing of the patterned Ni further highlight the control of channel lengths from ca.

88 50 nm (Fig. 2c) to 500 and 2000 nm (Supplementary Fig. 2c,d). Measured channel lengths and

89 ROCs were found to be consistent with those designed (Supplementary Fig. 3). Etching of the Ni

90 release layer produces arrays of probes, including single U-NWFET probes (Fig. 2d) and

91 multiple U-NWFET devices on a single probe arm (Supplementary Fig. 2e) where the active U-

92 NWFET sensor elements are oriented upwards away from the substrate.

93   Electrical transport studies in air and aqueous solution were carried out to characterize

94 the sensor properties. Current versus drain-source voltage ($I - V_{ds}$) measurements on devices

95 with channel lengths of ca. 50, 500, and 2000 nm (Fig. 2e-g; N=10, each channel length) in the

96 dry state yield average conductances of 3.3 ± 0.6, 0.7 ± 0.2 and 0.3 ± 0.1 μS, respectively. In

97 addition, conductance versus water-gate voltage (V_g) measurements in aqueous solution (Fig. 2h-

98 j) yield average transconductances of 5.4 ± 1.3, 2.3 ± 0.7 and 0.9 ± 0.3 μS/V for 50, 500 and

99 2000 nm channel lengths, respectively. The probe transconductance versus ROC ($0.75 - 2.0$ μm)

100 for devices with 50, 500 or 2000 nm FET channels (Supplementary Fig. 4 and Supplementary

101 Table 1) show that transconductance does not significantly vary as a function of ROC in our

102   designed strain range (Supplementary Table 2). The conductance and transconductance results

103   for the U-NWFETs are roughly consistent with the expected inverse relationship to the channel

104   length. Last, the transconductance and measured noise values yield an estimate for signal

105   detection sensitivity (3 standard deviations) of 0.90 ± 0.60, 1.2 ± 0.9 and 1.9 ± 0.9 mV for 50,

106   500 and 2000 nm channel lengths, respectively, which should allow detection of typical 1-10 mV

107   subthreshold activities of neurons[2].

Near full amplitude intracellular recordings

109   With these characterization results, we first asked whether ultrasmall U-NWFET probes

110   could record full amplitude intracellular action potentials from primary neurons. First, a single

111   U-NWFET probe with ca. 50 nm FET length and 0.75 μm ROC was used to sequentially

112   measure six independent dorsal root ganglion (DRG) neurons (Methods, Supplementary Fig. 5),

113   where the probe was not remodified with lipid between the sequential measurements

114   (Supplementary Fig. 6). In each trace, we observe a drop in the baseline potential upon initial

115   cell contact (Fig. 3a). Subsequently, either sparse peaks (Cells 1,3,6) or periodic peaks (Cells

116   2,4,5) are observed with amplitude of 60-100 mV and signal-to-noise ratios of 115 ± 29. For

117   each cell, the recorded potentials have consistent shape and duration, and characteristic single

118   peaks recorded from the 6 cells are shown in Fig. 3b. An additional set of data recorded from two

119   DRG neurons without spontaneous firing properties showed a voltage drop (Supplementary Fig.

120   7a), or one single peak followed by a voltage drop (Supplementary Fig. 7b) during device

121   penetration. Following the initial recording, we observed a gradual decrease in the peak

122   amplitude as well as a positive shift in the baseline potential (Fig. 3c, d and Supplementary Fig.

123   7).

124   These recordings highlight several key features. First, the waveforms, amplitudes, firing

125   patterns and signal-to-noise ratio of the peaks are similar to our patch-clamp recordings of

126   similarly cultured DRG neurons (Supplementary Fig. 8) and are consistent with the reported

127   heterogeneity of spontaneously firing DRG action potential waveforms and spike patterns[23].

128   These data thus indicate that the ultrasmall U-NWFETs with biomimetic phospholipid

129   modification can obtain high resistance membrane seals, achieve direct access to the cell interior,

130   and yield faithful recording of the intracellular potential. Notably, the data recorded from some

131   DRG neurons exhibit characteristics consistent with mechanosensitive properties[24], including an

132   increase in action potential firing rate (Fig. 3c,d) and firing of a single action potential

133   (Supplementary Fig.7b) during formation of the device/cell junction. A limitation of the

134   recording is, however, the shift in baseline and decrease in recorded action potential amplitude at

135   later times (e.g., Fig. 3c). We suggest that these changes are due to either an elastic response

136   from the cytoskeleton, which gradually pushes the probe out of the cell as suggested in other

137   intracellular chemical delivery experiments[25], or mechanical instability of the measurement

138   setup.

139   Given the high signal-to-noise for our measurements, we asked whether it was possible to

140   observe subthreshold activity. Notably, close examination of a representative trace from a cell

141   with irregular firing pattern (Fig. 3d) shows subthreshold features, including a single ca. 5 mV

142   peak (Fig. 3e(i)) and a series of three small peaks (Fig. 3e(iii)) immediately prior to the initiation

143   of an action potential, as well as a ca. 3 mV peak not associated with an action potential spike

144   (Fig. 3e(ii)); we recorded similar results with patch-clamp (blue triangles, Supplementary Fig. 8).

145   Previous multi-patch-clamp studies have reported comparable subthreshold signals and attributed

146   them to excitatory postsynaptic potentials in which a presynaptic cell triggers the firing of the

7

147   postsynaptic cell[2,26]. This suggests that our U-NWFET devices can measure biologically relevant

148   subthreshold signals and could be used for future studies of neural connections and synaptic

149   activity.

150   After achieving neuronal intracellular recording, we asked whether the U-NWFET probes

151   could be generalized to other electrogenic cells. To answer this question, we cultured human

152   induced pluripotent stem cell-derived cardiomyocytes (HiPSC-CMs) (Methods). Contact of a

153   HiPSC-CM and a U-NWFET probe with ca. 50 nm FET length and 0.75 μm ROC

154   (Supplementary Fig. 9a,b) initially yielded a ca. 25 mV drop in the baseline, followed by

155   periodic ca. 50 mV positive waveforms with a sharp rising phase (< 50 ms), slow falling phase

156   (ca. 400 ms) and frequency of 1.25 ± 0.04 Hz. The second measurement of the same cell resulted

157   again in a drop in the baseline potential and initial ca. 50 mV positive waveforms with

158   frequencies 1.23 ± 0.02 Hz (Supplementary Fig. 9c,d). Notably, the waveform frequency,

159   amplitude and shapes during the first and the second entry remain similar and are consistent with

160   reported cardiac action potentials[27], suggesting that the U-NWFET probe is also able to record

161   the intracellular potential of cardiac cells, and that the internalization process is minimally

162   invasive.

163   **Effect of nanowire geometry and sensor size on intracellular recording**

164   We first investigated geometry effects by fabricating probe arrays with ROCs ranging

165   from 0.75 μm to 2.0 μm (Fig. 4a, Supplementary Fig. 10) with fixed ca. 50 nm sensor sizes,

166   carrying out ca. 30 measurements for each ROC from both DRG neurons and HiPSC-CMs. For

167   DRG neurons, representative intracellular/intracellular-like recordings were obtained by probes

168   with 1 μm and 1.5 μm ROC (Fig. 4b, c), showing maximum action potential amplitudes of ca. 35

169   mV and 12 mV respectively. The distribution of maximum recording amplitudes from both cell

8

170 types (Fig. 4d,e) shows the average values for DRG/HiPSC-CM cells and number of successful

171 recordings (out of ca. 30 measurements) of 34±30 (N=24)/34±14 (N=31), 19±15 (N=25)/31±9

172 (N=6) and 16±7 (N=2)/21±9 (N=7) mV for 0.75, 1.0 and 1.5 μm ROC, respectively.

173 Interestingly, the 2.0 μm ROC probes did not yield successful recordings on both cell types,

174 indicating that increasing ROC correlates with lower recorded maximum amplitudes.

175 Measurement of device transconductance (Supplementary Fig. 11) and SEM images

176 (Supplementary Fig. 12) indicate that device characteristics do not change following

177 measurement.

178   Second, we studied how sensor size affects recording by fabricating U-NWFETs with

179 channel lengths of 500 nm and 0.75 μm ROC (Supplementary Fig. 10). Measurements made on

180 both DRG neurons and HiPSC-CMs showed 8±8 (N=7) and 23±13 mV (N=10) maximum

181 intracellular action potential amplitudes, respectively (Fig. 4f). Furthermore, U-NWFETs with

182 channel lengths of ca. 2000 nm and ROC of either 1.0 μm or 1.5 μm yielded maximum

183 amplitudes of 21±12 mV (N=5, blue circles) and 8.0 mV (N = 1, yellow circle), respectively

184 (Fig. 4g). Some of the 1.5 μm ROC, 2000 nm channel U-NWFETs recorded negative spikes with

185 maximum amplitudes of 4 ± 1 mV (N = 4, red triangles), while no successful recordings were

186 achieved on DRG cells with 2000 nm channel probes. A representative trace showing negative

187 spikes from a HiPSC-CM (Fig. 4h) highlights their periodic negative short < 3ms duration that

188 contrast a representative intracellular recording[27] obtained from a HiPSC-CM using 0.75 μm

189 ROC, 50 nm U-NWFET (Fig. 4i). The above data show that reducing the ROC and FET channel

190 length has a statistically significant correlation with the increases in both the maximum measured

191 action potential amplitudes and number of successful recordings (Supplementary Table 3). At the

192 most extreme limit, devices with 2 μm ROC no longer record action potentials, although devices

193   with 1.5 μm ROC and 2000 nm channel lengths recorded waveforms characteristic of

194   extracellular signals[27,28]. We hypothesize that the observed increase in recording amplitude with

195   decreasing ROC and channel length is not solely from physical interactions between the device

196   and the cell but also a consequence of reported results demonstrating that nanoscale curvature

197   can induce activation of endocytosis and related biological pathways.[17-20, 29] Our studies indicate

198   that using nanoscale topography to enhance device uptake is critical for developing tools that

199   faithfully capture intracellular action potential features.

200   We further examined the relationship between U-NWFET device ROC and channel

201   length and the intracellular recording duration. For both DRG neurons and HiPSC-CMs, there

202   was no significant difference (p-value>0.05) in recording duration with ROC (Supplementary

203   Fig. 13, Supplementary Table 4). Additionally, we observed that increasing channel lengths

204   showed no difference in recording duration in the DRG cells (p-value>0.05), while for the

205   HiPSC-CMs channel length increasing from 50 nm to 500 nm for the 0.75 μm ROC and from 50

206   nm to 2000 nm for the 1.0 μm ROC U-NWFET resulted in a statistically significant (p-

207   values=0.007,0.027 respectively) increase in recording duration (Supplementary Fig. 13,

208   Supplementary Table 4). The lack of correlation between ROC and recording distribution

209   suggests loss of intracellular access is related to curvature independent factors. We attribute the

210   observed increased recording duration for longer channel lengths for HiPSC-CMs to the higher

211   probability of maintaining a partially internalized configuration during cell contraction-induced

212   instabilities. Recordings obtained on DRG neurons have shorter duration than HiPSC-CMs,

213   possibly reflecting reported differences in cell membrane mechanical properties as neuron

214   membranes are generally less fluidic than those of cardiac cells[30].

215   Finally, we ask whether deterministic fabrication with size and geometry control could

216   enable multisite intracellular recording within a single cell using two U-NWFETs on one probe

217   arm, recording from cell networks using independent U-NWFET probes, and/or simultaneous

218   measurement of intracellular/extracellular action potentials from a single cell by two U-NWFETs

219   with different ROC and channel lengths (Fig. 5a). First, a single DRG neuron soma was brought

220   into contact with a pair of U-NWFETs (each with ca. 50 nm channel and 0.75 μm ROC)

221   separated by 2 μm on one probe arm. The simultaneously recorded intracellular action potential

222   amplitudes (Fig. 5b(i)) exhibited values of 46 and 28 mV from the two U-NWFETs. The

223   derivative of two action potentials signals (Fig.5b(ii)) and overlay of the two traces scaled to the

224   same peak amplitudes (Supplementary Fig. 14a,b) shows that the peaks coincide with each other,

225   indicating there is no discernible delay or waveform difference observed in the soma between the

226   two channels.

227   Second, a layer of cultured HiPSC-CMs was brought into contact with paired U-

228   NWFETs on the same probe arm (2 μm separation) and a third single U-NWFET probe

229   separated by 350 μm from the paired probe (all three U-NWFETs with ca. 50 nm channel and

230   0.75 μm ROC). The paired probe recorded the intracellular action potential within one cell with

231   action potential amplitudes 54 mV / 47 mV (Fig. 5c(i)) in the two channels, while the third probe

232   simultaneously recorded from another cell with amplitude of 62 mV (Fig. 5c(ii)). Comparison of

233   the time derivatives (Fig. 5c(iii)) showed no discernible delay in the paired channels, while there

234   was a ca. 6 ms delay between paired and single probes. This delay time and probe separation

235   yield a signal propagation speed of ~5.8 cm/s, which agrees with that reported in the literature[31].

236   Overlay of the action potentials (Supplementary Fig. 14c,d) shows good agreement in the rising

237   phase, and small deviations in the repolarization phase which can be attributed to different

238   changes in the two U-NWFET/cell junctions as a result of mechanical contraction[32].

239   Third, paired U-NWFETs containing one ca. 50 nm FET with 0.75 μm ROC and one ca.

240   2000 nm FET with 1.5 μm ROC on a single probe arm with 2 μm separation were fabricated and

241   brought into contact with a HiPSC-CM (Fig. 5d). The channel with the ca. 0.75 μm ROC, 50 nm

242   FET measured waveforms of ca. 50 mV characteristic of intracellular cardiac action potentials

243   (Fig. 5d(i)), while the channel with the 2.0 μm ROC, ca. 2000 nm FET measured sharp

244   downward spikes of ca. 2 mV and <5 ms duration characteristic of extracellular cardiac action

245   potentials (Fig. 5d(ii)). Close examination of the rising phase and derivative of the intracellular

246   trace in comparison to the extracellular trace (Fig 5d(iii)), shows that the measured extracellular

247   signal is dominated by a downward peak at the same time as the upwards phase of the action

248   potential. Extracellular waveforms measured using metal electrodes show increasing potential

249   from capacitive coupling with the intracellular space, which should be aligned with the time

250   derivative of the intracellular signal[28,33], followed by a decrease from inward Na^+ current during

251   action potential firing[33]. Our observed monophasic negative waveform suggests the small size of

252   our recording element decreases capacitive coupling with the interior of the cell so that only

253   local potential changes derived from inward Na^+ currents are observed. Furthermore, previous

254   reports of simultaneous extracellular and intracellular measurement required separate patch

255   clamp and metal electrode array recording systems which can introduce complications such as

256   spatial mismatch of recording sites and difficulty in temporal synchronization[28,33]. In comparison,

257   our multiplexed measurement strategy provides more localized information to correlate

258   extracellular and intracellular action potentials.

259   Last, we demonstrate the scalability of our U-NWFET devices by fabricating six device

260   regions containing 135 working single or multi U-NWFET devices (out of 168 addressable

261   device sites) on a 76 mm wafer (Supplementary Fig. 15a,b). For typical cell experiments, the

262   wafer is subsequently 'diced' to yield six chips that are individually mounted on printed circuit

263   boards (Supplementary Fig. 5a). Separate measurements from HiPSC-CMs for each of the 6 chip

264   device arrays yielded intracellular signal from at least 8 devices for each chip (Supplementary

265   Fig. 15c). In one device array, we designed a series of probes containing 1-4 nanowires per probe

266   arm (Supplementary Fig. 16a,b), and show simultaneous recording of action potentials in 10

267   channels from 4 separate cells (Supplementary Fig. 16c). These experiments validate the

268   potential for using our U-NWFET probes for multiplexed recording to study the

269   electrophysiology of cell networks.

270   **Conclusions**

271   In summary, we have demonstrated that the scalable ultrasmall U-NWFET probe arrays

272   fabricated using deterministic shape-controlled nanowire assembly and selective spatially-

273   defined solid-state semiconductor-to-metal transformation have the capability to record full

274   amplitude intracellular action potentials from primary neurons and other electrogenic cells, and

275   the capacity for multiplexed recordings. These new studies complement other efforts from

276   several groups focused on developing solid-state nanodevices for cell electrophysiology. While

277   our number of recording channels is limited compared to hundreds of channels demonstrated in

278   electrode array-based strategies[12,14], it is notable that our U-NWFETs show the capability to

279   record full-amplitude intracellular actions potentials that are similar to patch-clamp recordings,

280   but now in a scalable format. This flexible device structure/fabrication approach has further

281   provided direct information about the relationship between recording amplitude as a function of

13

282   device curvature and size, and thus supports the developing "curvature hypothesis" relating

283   nanotopography to endocytosis and cytoskeleton dynamics[17]. One key challenge, encountered

284   both by U-NWFETs and other nanodevices, is the long-term stability of the intracellular

285   recording. We hypothesize that future studies exploring either (1) chemical anchoring via surface

286   functionalization with groups that can bind to the actin cytoskeletal localized near highly curved

287   membranes[17,18,25] or (2) physical anchoring using spicule mesostructures[34] and/or modulation of

288   nanowire morphology[29] to increase the physical detachment force could improve the stability of

289   the intracellular device configuration. Supporting the potential of these proposed directions,

290   previous experiments indicate that functionalized free-standing nanowires can remain in the

291   interior of neurons for at least several hours[35]. More generally, this deterministic nanowire-based

292   fabrication strategy can be incorporated into other platforms, such as free-standing probes[16],

293   which allow precise targeting of individual cells or subcellular structures, and mesh

294   electronics[36,37] for in-vivo measurements.

295 **References**

296 1.   Chen, R., Canales, A. & Anikeeva, P. Neural recording and modulation technologies. *Nature Rev.*
297   *Mater.* **2**, 16093 (2017).

298 2.   Spira, M.E. & Hai, A. Multi-electrode array technologies for neuroscience and cardiology. *Nature*
299   *Nanotech.* **8**, 83-94 (2013).

300 3.   Kruskal, P.B., Jiang, Z., Gao, T. & Lieber, C.M. Beyond the patch clamp: nanotechnologies for
301   intracellular recording. *Neuron* **86**, 21-24 (2015).

302 4.   Savtchenko, L.P., Poo, M.M. & Rusakov, D.A. Electrodiffusion phenomena in neuroscience: a
303   neglected companion. *Nature Rev. Neurosci.* **18**, 598 (2017).

304 5.   Hamill, O.P., Marty, A., Neher, E., Sakmann, B. & Sigworth, F.J. Improved patch-clamp
305   techniques for high-resolution current recording from cells and cell-free membrane patches.
306   *Pflug. Arch. Eur. J. Phy.* **391**, 85-100 (1981).

307 6.   Martina, M. & Taverna, S. Patch-clamp methods and protocols, Edn. 2nd. (Humana Press, New
308   York; 2014).

309 7.   Jiang, Y.W. et al. Rational design of silicon structures for optically controlled multiscale
310   biointerfaces. *Nature Biomed. Eng.* **2**, 508-521 (2018).

311 8.   Parameswaran, R. et al. Photoelectrochemical modulation of neuronal activity with free-standing
312   coaxial silicon nanowires. *Nature Nanotech.* **13**, 260-266 (2018).

313 9.   Abbott, J., Ye, T.Y., Ham, D. & Park, H. Optimizing nanoelectrode arrays for scalable
314   intracellular electrophysiology. *Accounts Chem. Res.* **51**, 600-608 (2018).

315 10. McGuire, A.F., Santoro, F. & Cui, B.X. Interfacing cells with vertical nanoscale devices:
316   applications and characterization. *Annu. Rev. Anal. Chem.* **11**, 101-126 (2018).

317 11. Spira, M.E., Shmoel, N., Huang, S.H.M. & Erez, H. Multisite attenuated intracellular recordings
318   by extracellular multielectrode arrays, a perspective. *Front. Neurosci.* **12**, 212, (2018).

319 12. Abbott, J. et al. CMOS nanoelectrode array for all-electrical intracellular electrophysiological
320   imaging. *Nature Nanotech.* **12**, 460-466 (2017).

321 13. Dipalo, M. et al. Intracellular and extracellular recording of spontaneous action potentials in
322   mammalian neurons and cardiac cells with 3D plasmonic nanoelectrodes. *Nano Lett.* **17**, 3932-
323   3939 (2017).

324 14. Dipalo, M. et al. Plasmonic meta-electrodes allow intracellular recordings at network level on
325   high-density CMOS-multi-electrode arrays. *Nature Nanotech.* **13**, 965-972 (2018).

326 15. Tian, B.Z. et al. Three-dimensional, flexible nanoscale field-effect transistors as localized
327   bioprobes. *Science* **329**, 830-834 (2010).

328 16. Qing, Q. et al. Free-standing kinked nanowire transistor probes for targeted intracellular
329   recording in three dimensions. *Nature Nanotech.* **9**, 142-147 (2014).

330 17. Lou, H.Y., Zhao, W.T., Zeng, Y.P. & Cui, B.X. The role of membrane curvature in nanoscale
331   topography-induced intracellular signaling. *Accounts of Chem. Res.* **51**, 1046-1053 (2018).

332 18. Zhao, W.T. et al. Nanoscale manipulation of membrane curvature for probing endocytosis in live
333   cells. *Nature Nanotech.* **12**, 750-756 (2017).

334 19. Iversen, L., Mathiasen, S., Larsen, J.B. & Stamou, D. Membrane curvature bends the laws of
335   physics and chemistry. *Nature Chem. Biol.* **11**, 822-825 (2015).

336 20. Kaksonen, M. & Roux, A. Mechanisms of clathrin-mediated endocytosis. *Nature Rev. Mol. Cell*
337   *Bio.* **19**, 313-326 (2018).

338 21. Zhao, Y. et al. Shape-controlled deterministic assembly of nanowires. *Nano Lett.* **16**, 2644-2650
339   (2016).

340 22. Wu, Y., Xiang, J., Yang, C., Lu, W. & Lieber, C.M. Single-crystal metallic nanowires and
341   metal/semiconducotor nanowire heterostructures. *Nature* **430**, 61-65 (2004).

342 23. Study, R. E., & Kral, M. G. Spontaneous action potential activity in isolated dorsal root ganglion
343   neurons from rats with a painful neuropathy. *Pain* **65**, 235-242 (1996).

344 24. Delmas, P., Hao, J., & Rodat-Despoix, L. Molecular mechanisms of mechanotransduction in
345   mammalian sensory neurons. *Nature Rev. Neurosci.* **12**, 139-153 (2011).

346 25. Aalipour, A., Xu, A.M., Leal-Ortiz, S., Garner, C.C. & Melosh, N.A. Plasma membrane and actin
347   cytoskeleton as synergistic barriers to nanowire cell penetration. *Langmuir* **30**, 12362-12367
348   (2014).

349 26. Cossell, L. et al. Functional organization of excitatory synaptic strength in primary visual cortex.
350   *Nature* **518**, 399–403 (2015).

351 27. Burridge, P.W. et al. Chemically defined generation of human cardiomyocytes. *Nature Methods*
352   **11**, 855-860 (2014).

353 28. Sanders, K.M., Ward, S.M. & Hennig, G.W. Problems with extracellular recording of electrical
354   activity in gastrointestinal muscle. *Nature Rev. Gastro. Hepat.* **13**, 731-741 (2016).

355 29. Dipalo, M. et al. Cells adhering to 3D vertical nanostructures: cell membrane reshaping without
356   stable internalization. *Nano Lett.* **18**, 6100–6105 (2018).

357 30. Dietschy, J. M., & Turley, S. D. Thematic review series: brain Lipids. Cholesterol metabolism in
358   the central nervous system during early development and in the mature animal. *J. Lipid Res* **45**,
359   1375-1397 (2004).

360 31. Zhu, H.Q. et al. Two dimensional electrophysiological characterization of human pluripotent
361   stem cell-derived cardiomyocyte system. *Sci. Rep.* **7**, 43210 (2017).

362 32. Woodcock, E. A., & Matkovich, S. J. Cardiomyocytes structure, function and associated
363   pathologies. *Int. J. Biochem. Cell Biol*, **37**, 1746-1751 (2005).

364 33. Gold, C., Henze, D.A., Koch, C. & Buzsáki, G. On the origin of the extracellular action potential
365   waveform : a modeling study. *J. Neurophysiol.* **95**, 3113-3128 (2006).

366 34. Luo, Z. et al. Atomic gold – enabled three-dimensional lithography for silicon mesostructures.
367   *Science*, **348**, 1451–1455 (2015).

368 35. Lee, J.H., Zhang, A.Q., You, S.S. & Lieber, C.M. Spontaneous internalization of cell penetrating
369   peptide-modified nanowires into primary neurons. *Nano Lett.* **16**, 1509-1513 (2016).

370 36. Fu, T.M. et al. Stable long-term chronic brain mapping at the single-neuron level. *Nature*
371   *Methods* **13**, 875-882 (2016).

372 37. Hong, G.S. et al. A method for single-neuron chronic recording from the retina in awake mice.
373   *Science* **360**, 1447-1451 (2018).

374

379

380 **Author contributions**

381 Y.Z., S.S.Y. and C.M.L. conceived and designed the experiments, Y.Z., S.S.Y., and A.Z.

382 performed the experiments and analyzed the data, Y.Z., S.S.Y., A.Z and C.M.L. co-wrote the

383 paper. All authors discussed the results and commented on the manuscript.

384

385 **Additional information**

386 Supplementary information is available in the online version of the paper. Reprints and

387 permissions information is available online at www.nature.com/reprints. Correspondence and

388 requests for materials should be addressed to C.M.L (cml@cmliris.harvard.edu).

389

390 **Competing financial interests**

391 The authors declare no competing financial interests.

Figure captions:

Figure 1 | Ultrasmall U-shaped nanowire field effect transistor probe as a new approach for

394   **electrophysiology. a**, Schematics of intracellular recording by a U-NWFET probe. The location,

395   size, geometry of each probe and the sensor size can be well modulated by deterministic shape-

396   controlled nanowire transfer technique and spatially-defined transformation of Si nanowire

397   segments to NiSi, respectively. **b**, Schematics of two possible probe-cell interfaces: (**i**)

398   Internalization and high resistance seal of short-channel U-NWFET to the cell membrane enables

399   high amplitude recording. The sensitive p-type Si NWFET region and the metallic NiSi region

400   on U-shaped nanowire are marked with red and silver respectively. Nanowire is shown modified

401   with phospholipid. (**ii**) Partial sealing/internalization of U-NWFET with longer channel

402   length/ROC results in attenuated intracellular-like action potential recording.

403   **Figure 2 | Fabrication and characterization of U-shaped nanowire field effect transistor**

404   **probes. a**, Schematics of device fabrication. (**i**) Assembly of U-shaped nanowires devices on Ni

405   sacrificial layer and bottom Si_3N_4 passivation layer, and electrical contacts to the transferred U-

406   shaped nanowires are made via deposition of Cr/Au/Cr (1.5/60/60 nm) metal interconnects,

407   where the relative Cr/Au/Cr thicknesses yield a built-in strain that bends up the probe upon

408   release;(**ii**) Deposition of top Si_3N_4 passivation layer and Ni diffusion layer followed by rapid

409   thermal annealing to transform the Si nanowire segments underneath and adjacent to the Ni

410   diffusion layer to NiSi, and thus generate a local FET at the tip of the U-shaped nanowire; (**iii**)

411   Probes bending upward after etching the Ni diffusion and sacrificial layers. **b**, Optical image of

412   three devices following deposition of metal interconnects and before deposition of nickel

413   diffusion layer. Inset is the zoom-in view showing that a U-shaped nanowire is deterministically

414   transferred to the device tip. Scale bar 20 μm. **c**, SEM image of device after Ni diffusion. Scale

415   bar 500 nm. Inset is a zoom-in SEM image of the dashed region showing the resulting local FET

416   at the U-shaped nanowire tip. Scale bar 50 nm. Imaging with backscattered electrons (BSE)

417   shows the Si (dark region) and NiSi (bright region) distribution on the U-shaped nanowire. Scale

418   bar 50 nm. **d**, Optical image of bend-up device array in water. Scale bar 20 μm. **e-g**, Current

419   versus drain-source voltage (V_{ds}) traces for 10 devices in the dry state for (**e**) ca. 50 nm, (**f**) ca.

420   500 nm, and (**g**) ca. 2000 nm channel lengths. Insets show SEM images taken using BSE mode

421   of the local FET following removal of Ni layer. Scale bars: (**e**) 50 nm, (**f**) 0.5 μm, (**g**) 0.5 μm. **h-**

j, (Left) Conductance versus reference water-gate potential (V_g) recorded from one representative device for each channel length ((**h**) ca. 50 nm, (**i**) ca. 500 nm, and (**j**) ca. 2000 nm) in Tyrode's solution. (Right) Box and whisker plot showing distribution (N=10) of transconductances for devices of each channel length gated by a reference electrode in Tyrode's solution. The blue triangle indicates the mean of the transconductances and the top and bottom edges of the box indicate the upper/lower quartiles respectively. The error bars reflect ±1 s.e.m.

Figure 3 | Intracellular recording of dorsal root ganglion neurons neuron by ultrasmall U-shaped nanowire field effect transistor probe. a, Intracellular action potentials recorded sequentially from 6 independent neurons using the same U-NWFET probe without re-modification. The numbering of the cells indicates the order in which the measurements occurred. The probe has ca. 50 nm FET channel length and 0.75 μm ROC. **b,** The summary of recorded action potentials from the 6 different cells in panel **a** in chronological order. Maximum signal amplitude remains similar between these measurements, showing that the probe is highly reusable. The signal-to-noise of these recordings is 115 ± 29 (N=6). **c,** Intracellular recording trace from a cell with regular firing pattern showing a gradual increase in baseline potential and decrease in action potential amplitude. **d,** Representative trace from a cell with irregular firing pattern where subthreshold activities appear in regions outlined by blue dashed lines. **e,** Zoom in regions of three different areas from panel **d** showing different types of subthreshold activities, highlighted by the red arrows and blue dashed regions.

Figure 4 | Effect of size and geometry of U-shaped nanowire field effect transistor probes on electrophysiological recordings. a, Optical image of U-NWFET probes with different ROC before deposition of Ni diffusion layer (**i**) 0.75 μm, (**ii**) 1 μm, (**iii**) 1.5 μm and (**iv**) 2 μm. **b,c,** Intracellular/intracellular-like recording from DRG neuron by ca. 50 nm FET channel length probe with (**b**) 1 μm and (**c**) 1.5 μm ROC. Insets are the zoom-in view of selected action potentials. **d-e,** Plot of maximum recorded spike amplitude of recorded action potentials from DRG neurons (**d**) and HiPSC-CMs (**e**) versus ROC with fixed ca. 50 nm FET length. Coloured bars indicate the maximum spike amplitudes measured in the given data set. The statistical significance shown above obtained by comparing the datasets below the ends of the black line using the student's t-test. ****: p-value < 0.0001. The blue letters 'b', 'c' and 'i' highlight the data points from panels **b**,**c**,**i**. **f,** Scatter plot of maximum recorded spike amplitude of DRG

452 neurons **(i)** and HiPSC-CMs **(ii)** for ca. 500 nm FET channel lengths with 0.75 μm ROC. The

453 statistical significance **** shown in **(i)** and **(ii)** obtained by comparing the datasets in **(i)** and **(ii)**

454 with datasets of ROC 0.75 μm in **(d)** and **(e)** respectively. **g**, Plot of maximum recorded spike

455 amplitude of HiPSC-CMs with ca. 2000 nm FET channel. Blue circles represent intracellular

456 data recorded from U-NWFETs with 1.0 μm ROC and yellow circles represent intracellular data

457 recorded from U-NWFET with 1.5 μm ROC. Red triangles represent extracellular data recorded

458 from U-NWFETs with 1.5 μm ROC. The letter h represents the data point for the trace shown in

459 panel **h**. Note that for all scatter plots, ca. 30 measurements were attempted for each U-NWFET

460 channel length and ROC, and recordings which did not result in measurement of

461 intracellular/intracellular-like or extracellular action potentials were considered as 0 mV max

462 spike amplitude and not shown for clarity but are summarized in Supplementary Table 3. **h**,

463 Extracellular recording from HiPSC-CMs by ca. 2000 nm FET channel length probe with 1.5 μm

464 ROC. Inset is the zoom-in of the highlighted spike. **i**, Intracellular recording from HiPSC-CMs

465 by ca. 50 nm FET channel length probe with 0.75 μm ROC.

466 **Figure 5 | Multiplexed electrophysiological recording by U-shaped nanowire field effect**

467 **transistor probes. a**, Schematics of **(i)** simultaneous multisite intracellular recording from single

468 neuron by paired U-NWFETs on one probe arm, **(ii)** multiplexed intracellular recording from

469 different cells by U-NWFETs on different probe arms, and **(iii)** simultaneous

470 intracellular/extracellular recording from one cell by paired U-NWFETs on one probe arm. **b**, **(i)**

471 simultaneous intracellular recording from one DRG neuron by two ca. 50 nm FETs with 0.75 μm

472 ROC on one probe arm with a 2 μm separation. **(ii)** the derivative of traces in dashed block

473 marked region. The vertical dashed guiding line indicates the time point of the first action

474 potential. No time delay is observed. **c**, multiplexed intracellular recording from two HiPSC-

475 CMs by **(i)** one paired U-NWFET probe and **(ii)** one single U-NWFET probe. **(iii)** the derivative

476 of marked region. Two probes arms are fabricated with a distance of 350 μm. **d**, simultaneous

477 intracellular/extracellular recording from one HiPSC-CM by **(i)** one ca. 50 nm FET with 0.75μm

478 ROC (red top, original intracellular signal; red bottom, derivative of intracellular signal) and **(ii)**

479 one ca. 2000 nm FET with 1.5 μm ROC on one probe arm with 2 μm separation. **(iii)** Closer

480 examination of the marked region.

481

Methods

Nanowire synthesis

Si nanowires (p-type) with 15 nm diameters were synthesized by a gold nanocluster-catalyzed vapour-liquid-solid growth method[21]. Growth substrates (15 x 60 mm^2 pieces of Si wafer with 600 nm thermal oxide, Nova Electronic Materials, Flower Mound, TX) were oxygen plasma cleaned (100 W, 2 min, 50 cubic centimetres per minute (sccm) O$_2$; PJ Plasma Surface Treatment System, Billerica, MA), treated with poly-L-lysine solution (0.1%, 150,000 – 300,000 g/mol, Ted Pella, Inc., Redding, CA) for 5 min, rinsed thoroughly with deionized (DI) water and dried with nitrogen. Then 1 mL of aqueous solution of 10 nm gold nanoparticles (Ted Pella, Inc., Redding, CA) with concentration of 1.9 x 10^{12}/particles/mL was dispersed[38] on the substrate for 2 min followed by thorough rinsing with DI water and drying with nitrogen (gold nanoparticle surface concentration: 0.01–0.04 particles/μm^2). The substrate was then placed into a home-built chemical vapour deposition reactor and the system was evacuated to a base pressure of 0.6 mTorr. Nanowires were synthesized at 430 °C at a total pressure of 40 Torr with gas flow rates of 2.5 sccm silane (SiH$_4$, 99.9999%, Voltaix, Branchburg, NJ) as the silicon reactant, 3.1 sccm diborane (B$_2$H$_6$, 100 p.p.m. in H$_2$, Voltaix, Branchburg, NJ) as the p-type dopant, and 60 sccm hydrogen (H$_2$, 99.999%; Matheson, Basking Ridge, NJ) as the carrier gas. Typical growth times of 1hr yielded nanowires with average lengths of ca. 50 μm.

U-NWFET probe array fabrication

Key steps involved in the fabrication of U-NWFET probe arrays are shown in Fig. 2 and Supplementary Fig. 1, with the key parameters as follows:

(**1**) LOR 3A (Microchem, Westborough, MA) and diluted S1805 (S1805: Thinner-P = 1:2 (vol : vol), Microchem, Westborough, MA) were spin-coated on a Si$_3$N$_4$/SiO$_2$-coated Si wafer (200 nm Si$_3$N$_4$, 100 nm SiO$_2$ on p-type Si, 0.005 Ω cm, or 600 nm thermal SiO$_2$ on n-type Si, 0.005 Ω cm, Nova Electronic Materials, Flower Mound, TX) and baked at 180 °C for 5 min and at 115 °C for 1 min respectively. The photoresist was patterned by photolithography (PL) with a Maskless aligner (MLA150, Heidelberg, Germany) and developed (MF-CD-26, MicroChem Corp., Newton, MA) for 30s. Following this PL process, a 60-nm thick Ni sacrificial layer was deposited by thermal evaporation (Sharon Vacuum Co. Inc., Brockton, MA), followed by a lift-off step (Remover PG, MicroChem Corp., Newton, MA). (Supplementary Fig. 1a) The size of the Ni sacrificial layer is designed to accommodate the size of the U-NWFET probe: 30 μm x 100 μm for single U-NWFET probes (Supplementary Fig. 1h(i)) or 90 μm x 100 μm for up to 4 U-NWFETs probes per bend-up probe arm (Supplementary Fig. 1h(ii)).

(**2**) The PL process in step 1 was repeated to define an 80 μm long bottom region for sputter deposition of 60 nm of Si$_3$N$_4$ passivation layer (Orion 3 Sputtering Systems, AJA International Inc., Scituate, MA). The

515   main body of Si$_3$N$_4$ passivation layer (75 μm long) was deposited on the Ni sacrificial layer with 5 μm

516   Si$_3$N$_4$ extending outside of the sacrificial region. (Supplementary Fig. 1b)

517   (**3**) LOR 1A (Microchem, Westborough, MA) and diluted S1805 (S1805: Thinner-P = 1:2 (vol : vol)) was

518   spin-coated and baked at 180 °C for 5 min and at 115 °C for 1 min, respectively. Then the PL process in

519   step 1 was repeated for defining arrays of trenches with shapes and ROCs as described in the main text.

520   (Supplementary Fig. 1c)

521   (**4**) Shape-controlled deterministic nanowire assembly was used to align disordered straight nanowires

522   into U-shaped arrays as described previously[21]. (Supplementary Fig. 1d) Briefly, a wafer with an array of

523   trenches was mounted onto a micromanipulator-controlled moveable stage, covered with mineral oil

524   (viscosity $v \approx 70$ mPa•s, #330760, Sigma-Aldrich, St. Louis, MO) as the lubricant, and then the nanowire

525   growth substrate was brought into contact with the target substrate with controlled contact pressure. The

526   target substrate was moved at a constant velocity of ca. 5 mm/min with respect to the fixed nanowire

527   growth substrate, and then the growth substrate was removed, and the target substrate rinsed with octane

528   (98%, Sigma-Aldrich, St. Louis, MO) to remove the lubricant. Estimations of the U-shaped nanowire

529   strain are calculated and shown in Supplementary Table 2.

530   (**5**) Aluminium oxide (Al$_2$O$_3$) was deposited directly after the nanowire assembly by atomic layer

531   deposition (ALD, S200, Cambridge NanoTech, Waltham, MA) with 1 cycle (1.4Å) at 80 °C to fix the U-

532   shaped nanowires on the bottom passivation layer and then all photoresist was removed in Remover PG.

533   (Supplementary Fig. 1e)

534   (**6**) Step 1 was repeated for simultaneously patterning electrical interconnects to the U-NWFET as well as

535   connects to large pads used as the input/output (I/O) region. Native oxide on the nanowire was etched by

536   buffered oxide etch (BOE, 7:1, Microchem, Westborough, MA) for 10s before thermal deposition of

537   asymmetrically strained metal Cr/Au/Cr (1.5/60/60 nm). The strained metal leads the U-NWFET probe to

538   bend off the wafer surface following etching of the sacrificial layer, like that described in previous

539   work[21].

540   (**7**) Step 2 was repeated to deposit 60 nm of Si$_3$N$_4$ as electrical passivation over exposed metal features

541   except for the I/O pad region. (Fig. 2b and Supplementary Fig. 1f).

542   (**8**) Electron-beam lithography (EBL) or PL was used to define the Ni diffusion region with shape and

543   position as described in the main text. Specifically, EBL was used for U-NWFET probe with ca. 50 nm

544   (Fig. 2c) and ca. 500 nm channel length (Supplementary Fig. 2c). For the EBL process, copolymer MMA

545   (EL6, Microchem, Westborough, MA) and polymethyl methacrylate (PMMA, 950-C2, Microchem,

546   Westborough, MA) were spin-coated and baked at 180 °C for 5 min sequentially. The resists were then

547   patterned with an EBL system (ELS-F125, Elionix, Japan) and developed (MIBK/IPA 1:1, MicroChem

548   Corp., Newton, MA) for 60 s. For U-NWFET probe with ca. 2000 nm channel length (Supplementary

549   Fig. 2d), the same PL process in step 1 can be used to define regions for Ni deposition. Native oxide on

550   the nanowire was removed by BOE for 10 seconds before deposition of 20 nm Ni via thermal

551   evaporation. After lift-off, the chip was annealed by Rapid Thermal Processor (RTP, 600xp, Modular

552   Process Technology, San Jose, CA) in forming gas (H_2:N_2 10:90) at 350 ^{o}C for 5min to transform Si

553   nanowire segments underneath and adjacent to Ni diffusion layer to nickel silicide[22], thereby generating a

554   localized sensing element. (Supplementary Fig. 1g)

555   (**9**) Polydimethylsiloxane (PDMS) was prepared by first pouring Sylgard 184 (Dow Corning, Inc,

556   Midland, Michigan) elastomer mixed in a 10:1 ratio of base to curing agent into a petri dish, and then

557   curing overnight at 55 °C in a convection oven. A PDMS chamber with ca. 20×30 mm^2 opening and ca.

558   0.5 cm sidewalls were cut from the cured PDMS and mounted around the device region using Kwik-Sil

559   silicone adhesive (World Precision Instruments, Sarasota, FL). A printed circuit board (PCB, UXCell,

560   Hong Kong, China) connector was then mounted adjacent to the I/O region of devices and then wire-

561   bonded to the U-NWFET probe I/O pads (Supplementary Fig. 5a). Probes were kept in dry-keeper

562   desiccator cabinet (H-B Instrument-Bel-Art, Wayne, NJ). Before electrical characterizations and/or

563   electrophysiological measurements, the Ni sacrificial layers and remaining Ni from the diffusion layer

564   were removed in nickel etchant (Nickel Etchant TFB, Transense, Danvers, MA) for 3 - 5mins, which

565   allowed release of these devices into three-dimensional bend-up structure (Fig. 2d and Supplementary

566   Fig. 1h). Following release, the devices were rinsed in DI water 5-10 times for 20 s each.

567   **Device Characterization**

568   Overview optical images of the measurement set-up and U-NWFET probe chip to instrument I/O were

569   acquired with an SLR digital camera (Canon U.S.A., Inc., Melville, NY) and higher resolution bright-

570   field optical images of individual U-NWFET probes and probe arrays were acquired by Olympus

571   BX50WI with Andor Luca EMCCD camera. High-resolution SEM images of nanowires, including

572   intermediate fabrication steps, were acquired by Zeiss Ultra Plus field emission SEM (Carl Zeiss,

573   Germany). A backscattered electron (BSE) detector was used to obtain high-resolution composition-

574   sensitive maps based on the electron elastic scattering difference of atomic number on the sample. U-

575   NWFET fabricated for characterization did not have Ni sacrificial layer to improve contrast during SEM

576   imaging. The BSE images show the silicon and nickel silicide segments on U-shaped nanowires: the

577   bright region indicates nickel/nickel silicide, and dark region indicates p-type Si.

578   For electrical characterization, one arm of the U-NWFET is considered as the source, and the other arm is

579   considered as the drain. A voltage, V_{ds} was applied between the source and drain of the U-NWFET, and

580   the resulting current, I_{ds} was measured. The electrical conductance (I_{ds}/V_{ds}) of the U-NWFET devices

581   were measured in the dry state by sweeping V_{ds} between -1 and 1 V and measuring I_{ds} using a homemade

582   battery powered 16-channel current preamplifier with bandwidth of 6 kHz which amplified the current

583 signal for recording using a 16-channel A/D converter (Axon Digidata 1440A; Molecular Devices, San

584 Jose, CA) controlled by pCLAMP 10.7 software (Molecular Devices). The I_{ds} - V_{ds} date were recorded in

585 air/dry state.

Surface Functionalization of U-NWFET probes

587 Phospholipid vesicles were prepared for use to functionalized U-NWFET probes in the following manner

588 similar to previous papers[15,16]: (1) 1,2-dimyristoyl-sn-glycero-3-phosphocholine (DMPC, Avanti Polar

589 Lipids Inc., Alabaster, Alabama) was suspended in chloroform (anhydrous, > 99%, Sigma-Aldrich, St.

590 Louis, MO) to a concentration of 20 mg/mL and mixed with 1% mass of 1-myristoyl-2-[12-[(7-nitro-2-

591 1,3-benzoxadiazol-4-yl)amino]dodecanoyl]-sn-glycero-3-phosphocholine (NBD-lipid, Avanti Polar

592 Lipids Inc. Alabaster, Alabama). (2) The solution of DMPC/NBD-lipid was then placed into a vacuum

593 desiccator for at least 6 hrs to evaporate off the chloroform. (3) The resulting powder was resuspended in

594 phosphate buffered saline (1x PBS, HyClone, South Logan, Utah) to concentration of 1 mg/mL and the

595 lipid solution was placed in a water bath at 37 °C for at least 2 hrs with periodic agitation using a vortex

596 mixer (30s every 20 minutes; Maxi Mix II, Barnstead/Thermolyne Corp, Dubuque TX) to ensure full

597 rehydration. (4) The resulting lipid solution was sonicated using a tip sonicator (25% amplitude, 10s/15s

598 pulse on/off, Branson Ultrasonics Sonifier S-450l, Branson Ultrasonics, Milford, CT) at ca. 37 °C for 2

599 hrs. (5) Following sonication, the lipid solution was sterile filtered (0.2 μm Acrodisc syringe filter, PN

600 4192, Pall Corporation, Port Washington, New York), and used within 1 hr of preparation.

601 Immediately prior to measurements, U-NWFET probe arrays with a mounted PDMS chamber

602 (Supplementary Fig. 5b) were incubated for 2 hr in 1.5 mL of the prepared lipid vesicle solution to allow

603 functionalization of U-NWFET as reported previously for other nanowire devices[15,16]. Following

604 incubation, the U-NWFET probe arrays were rinsed in Tyrode's solution (in mM, NaCl 155, KCl 3.5,

605 MgCl₂ 1, CaCl₂ 1.5, HEPES 10, D-glucose 10, pH 7.4 for DRG neurons, or NaCl 138, KCl 4, CaCl₂ 2,

606 MgCl₂ 1, Na₂HPO₄ 0.33, HEPES 10, glucose 10, pH 7.4 for HiPSC-CMs, all chemicals in Tyrode's

607 solution were purchased from Sigma-Aldrich, St. Louis, MO) 5-10 times for 20 s, ca. 3 mL each.

Device Characterization in Tyrode's Solution

609 Following phospholipid modification, electrical measurements were carried out in Tyrode's solution. The

610 electrical conductance of the U-NWFETs was continuously measured by recording the drain-source

611 current (I_{ds}) at a fixed source-drain DC bias between 0.1 - 0.2 V by the electronic measurement setup

612 mentioned above. The sensitivities (transconductance) were then obtained by sweeping an Ag/AgCl

613 reference electrode (2.0 x 4.0 mm, E-201, Warner Instruments, Hamden, CT) between -100 mV and 100

614 mV and measuring the corresponding linear change in U-NWFET conductance. The measured average (in

615 10 samples) conductance of U-NWFET for channel length ca. 50 nm, ca. 500 nm, ca. 2000 nm are 3.3 ±

616 0.6, 0.7 ± 0.2 and 0.3 ± 0.1 μS, with average sensitivity of 5.4 ± 1.3, 2.3 ± 0.7 and 0.9 ± 0.3 μS/V

617 respectively. An inverse relationship exists between conductance, and consequently transconductance,

618 and channel length, as expected from the relationship: ($G = \sigma A/L$), where G is the channel conductance, σ

619 is the electrical conductivity and A is the cross-sectional area of the wire and L is the channel length[39].

620 To estimate the noise level of the U-NWFETs devices, the conductance of the 10 devices for each channel

621 length was measured at using the Ag/AgCl reference electrode to fix the solution voltage at 0 for ca. 5 s.

622 The standard deviation of the measured conductance was used to obtain the noise for each device in uS.

623 Then, the transconductance of each device was used to convert the measured noise in uS into a value in

624 mV, and the resulting number is multiplied 3 to estimate the limit of detection as per convention.

625 Averaging the 10 values for limit of detection (in mV) for each channel length resulted in noise levels of

626 0.90 ± 0.60 mV, 1.2 ± 0.9 mV, 1.9 ± 0.9 mV for the ca. 50 nm, 500 nm, and 2000 nm devices

627 respectively.

628 **Preparation of flexible cell culture substrates**

629 A master mould for the culture substrate was first prepared by spin coating SU-8 2000.5 (Microchem,

630 Westborough, MA) onto a Si wafer and patterning repeating 3 μm wide lines with 3 μm spacing using PL.

631 After patterning, the master mould was hard baked on a hot plate at 180 °C for 2 hrs, and then silanized

632 with tridecafluoro-1,1,2,2- tetrahydrooctyl-1-trichlorosilane (Sigma-Aldrich, St. Louis, MO) for 2 hrs in a

633 vacuum desiccator, to enhance release of the PDMS template from the master mould[40].

634 Flexible PDMS cell culture substrates were prepared by spin coating Sylgard 184 elastomer mixed in a

635 10:1 ratio of base to curing agent onto the master mould at 250 rpm for 1 min. The PDMS on the master

636 mould was then cured in a convection oven set to 180 °C for 2 hrs, resulting in a thickness of ca. 220 μm

637 and cut into pieces with size of ca. 10×10 mm^2 for cell culture. Prior to cell culture, PDMS substrates

638 were autoclaved at 125 °C for 1 hr, treated by O_2 plasma (100 W, 2 min, 50 sccm O_2) and then washed in

639 75 % (v/v) solution of ethanol (200 proof, KOPTEC; King of Prussia, PA)/water for 1hr.

640 For DRG neuron culture, the PDMS was first functionalized with 40 μg/ml poly-D-lysine (Molecular

641 weight > 300,000 g/mol, Sigma-Aldrich, St. Louis, MO) in DI water for 1hr at room temperature. After

642 poly-D-lysine functionalization, PDMS was washed twice in DI water for 30 s each and air dried, and

643 then was functionalized with 20 μg/ml laminin (Thermo Fisher Scientific, Waltham, MA) in Leibovitz's

644 L-15 (Thermo Fisher Scientific, Waltham, MA) for 1 hr at room temperature. Laminin solution was

645 removed immediately before cell suspension was plated on PDMS.

646 For HiPSC-CM culture, the PDMS was functionalized sequentially with (1) 1% (3-

647 Aminopropyl)triethoxysilane (Sigma-Aldrich, St. Louis, MO) in 95 % (v/v) solution of ethanol/DI water

648 for 20 min at room temperature, followed by washing 3 times in ethanol for 30 s each, and 3 times in DI

649 water for 30 s each; (2) 2.5 % (v/v) Glutaraldehyde (Grade I, 50% in H_2O, Sigma-Aldrich, St. Louis,

650 MO)/water for 1 hr at room temperature, followed by washing 3 times in DI water for 30s each, and (3)

651 Geltrex Matrix (Thermo Fisher Scientific, Waltham, MA) at 37 °C for ca. 8 hrs. Geltrex solution was

652 removed immediately before cell suspension was plated onto the PDMS.

Cell culture

654 Dissociated DRG cells were prepared as described previously[35] and cultured in the CO_2 incubator

655 overnight before use. Cells that can spontaneously fire (e.g., Supplementary Fig. 8) were selected for

656 recording. HiPSC-CMs were cultured as described in the NCardia online protocol[41]. Cryogenically frozen

657 Cor.4U HiPSC-CM vials (Cor.4U $\geq$250k cells, Ncardia Group, Cologne, Germany) were thawed in 37 °C

658 water bath, and 0.5 mL of proprietary Cor.4U cell media (Ncardia group; Cologne, Germany) preheated

659 to 37 °C was added to the vial. The cell solution was then homogenized by gentle aspiration and seeded at

660 75 k cells/cm^2 to achieve confluency onto the prepared PDMS substrates. Immediately following cell

661 seeding, the cell culture was left at room temperature for 20 min to allow the solution to settle and ensure

662 an even distribution of cells. The cells were then cultured in a 5% CO_2, 37 °C incubator and the Cor.4U

663 cell media was first changed 6 hrs following plating. Subsequently, the media was changed every day and

664 the cells were used within 2 weeks following seeding, once a uniformly contracting layer was observed.

Electrophysiological recording with U-NWFET

666 The Ag/AgCl reference electrode is used to fix the extracellular Tyrode's solution voltage to 0 V for cell

667 measurements. A PDMS sheet with cultured DRG neurons or HiPSC-CMs was fixed upside down onto a

668 homebuilt vacuum wand mounted on a 40 nm step resolution x-y-z micromanipulator (MP-285, Shutter

669 Instruments) connected to a micromanipulator controller (MPC-200/ROE-200, Sutter Instruments) to

670 position the cells over and bring the cells into contact with the U-NWFETs (Supplementary Fig. 5c). The

671 Tyrode's solution was maintained at room temperature for the DRG neuron experiments and at ca. 37 °C

672 for the HiPSC-CM experiments. For longer (>3 minutes) HiPSC-CM intracellular recording

673 (Supplementary Fig. 9b, d), high pass filters were set to 0.4Hz, similar to that used by other groups[12,42,43].

Patch-clamp recording

675 Patch-clamp recording was performed at room temperature using Multiclamp 700B amplifier (Molecular

676 Devices) and Digidata 1440A Digitizer Acquisition System, controlled by pCLAMP 10.7 software

677 (Molecular Devices). Micropipettes were prepared using a micropipette puller (P-97, Sutter Instruments),

678 the pipette tip resistance ranged between 5–10 MΩ. DRG neurons were cultured on a glass coverslip with

679 the same modification as PDMS. Recording from DRG neurons was carried out in Tyrode's solution. The

680 micropipettes were filled with an internal solution consisting of (in mM): potassium L-aspartate 140,

681 NaCl 13.5, $MgCl_2$ 1.8, ethylene glycol-bis(2-aminoethylether)-N,N,N',N'-tetraacetic acid (EGTA) 0.09,

682 HEPES 9, phosphocreatine di(tris) salt 14, adenosine 5′-triphosphate (ATP) magnesium salt 4, guanosine
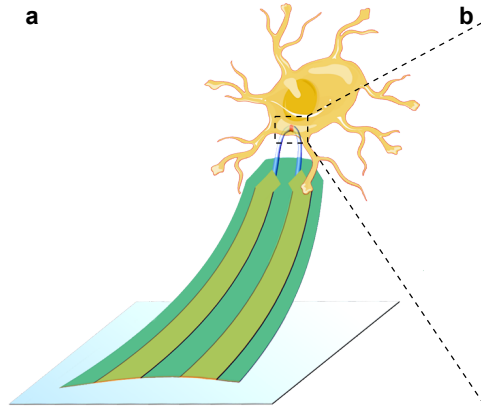
683   5'-triphosphate (GTP) tris buffered 0.3, pH 7.2 adjusted with KOH[6]. All chemicals in the internal solution

684   were purchased from Sigma-Aldrich, except GTP tris buffer, which was purchased from Thermo Fisher.

685

Data availability

687   The data that support the findings of this study are available from the corresponding author upon

688   reasonable request.

689

References

691   38. Patolsky, F., Zheng, G., & Lieber, C. M. Fabrication of silicon nanowire devices for ultrasensitive,
692   label-free, real-time detection of biological and chemical species. *Nature Protocols* **1**, 1711–1724
693   (2006).

694   39. Kittel, C. Introduction to solid state physics. 8th edn, (Wiley, 2005).

695   40. Minteer, S. D. Microfluidic techniques: reviews and protocols. Totowa, N.J., Humana Press. (2006)

696   41. NCardia, Cardiomyocytes User Manual,
697   https://ncardia.com/files/documents/manuals/PluricyteCardiomyocyte_Manual_v2.pdf

698   42. Shmoel, Nava, et al. Multisite electrophysiological recordings by self-assembled loose-patch-like
699   junctions between cultured hippocampal neurons and mushroom-shaped microelectrodes. *Scientific*
700   *reports* **6**, 27110 (2016).

701   43. Xie, Chong, et al. Intracellular recording of action potentials by nanopillar electroporation. *Nature*
702   *Nanotech.* **7**, 185–190 (2012).

a

b

i Cytoplasm

FET

Conducting nickel silicide

Extracellular fluid

ii Cytoplasm

FET

Conducting nickel silicide

a

i
- U-shaped Si nanowire
- Source
- Drain
- Bottom Si$_3$N$_4$
- Ni sacrificial layer
- Si substrate

ii
- Ni diffusion layer
- Top Si$_3$N$_4$

iii
- Bend-up nanoFET with modulated size
- Bend-up probe arm

e

f

g

h 50 nm

i 0.5 μm

j 2 μm

a (i) 0.75 μm (ii) 1 μm (iii) 1.5 μm (iv) 2 μm

b DRG neuron — 10 mV; inset 20 mV, 10 ms

c DRG neuron — 5 mV; inset 5 mV, 10 ms

d DRG — Max Spike Amplitude (mV) vs Radius of Curvature (μm): 0.75, 1.0, 1.5, 2.0; * , ****

e HiPSC-CM — Max Spike Amplitude (mV) vs Radius of Curvature (μm): 0.75, 1.0, 1.5, 2.0; ****, ****

f (i) DRG 500 nm FET 0.75 μm ROC ****; (ii) HiPSC-CM 500 nm FET 0.75 μm ROC ****

g 2000 nm FET — Max Spike Amplitude (mV); 1.0 μm ROC, 1.5 μm ROC, 1.5 μm ROC, EC

h HiPSC-CM, Extracellular — 1 mV; inset 2 mV, 5 ms

i HiPSC-CM, Intracellular — 20 mV